Twisted double ABC-stacked trilayer graphene with weak interlayer coupling

Sung Ju Hong [1,2,*] Donglei Wang,[1] Dirk Wulferding [3,4,5] Peter Lemmens [3] and Rolf J. Haug [1]

[1]*Institut für Festkörperphysik, Leibniz Universität Hannover, Hannover 30167, Germany*

[2]*Division of Science Education, Kangwon National University, Chuncheon 24341, Republic of Korea*

[3]*Institute for Condensed Matter Physics, Technische Universität Braunschweig, Braunschweig 38106, Germany*

[4]*Center for Correlated Electron Systems, Institute for Basic Science (IBS), Seoul 08826, Republic of Korea*

[5]*Department of Physics and Astronomy, Seoul National University (SNU), Seoul 08826, Republic of Korea*

(Received 16 November 2021; revised 8 April 2022; accepted 19 April 2022; published 2 May 2022)

Magnetotransport properties of single- and double-rhombohedral trilayer graphene (TLG) are studied. Double TLG is obtained by folding single TLG, yielding a twist angle of 4°. Raman spectroscopic measurements confirm ABC stacking order and the presence of interlayer coupling. The Landau fan diagram exhibits independently superimposed features of each constituent TLG, indicating weak interlayer coupling. As a result, we show that the current framework for twisted systems can be extended to TLG.

DOI: 10.1103/PhysRevB.105.205404

I. INTRODUCTION

Twisted bilayer graphene (tBLG) has been intensively investigated because various electronic transport phenomena can be obtained which are not observed in its constituent layer, monolayer graphene (MLG). Whereas at an early stage two independent electronic transport contributions at large twist angles were figured out [1–6], pronounced modifications of the electronic band structure related to the formation of superlattice structures have been observed at small twist angles later on [7–11]. Furthermore, emergent exotic phenomena (e.g., superconductivity and Mott insulator) were experimentally obtained at magic twist angles where enormous densities of states were formed due to flat bands [12,13]. As a result, tBLG paved the way for the field of twistronics where the additional degree of freedom (twist angle) is of significance to determine electronic properties in two-dimensional (2D) heterostructures [14].

The family of twisted systems recently expanded using Bernal-stacked bilayer graphene (BLG), where the electronic properties can be explained within the same framework as in tBLG [15–18]. Owing to the sensitivity to a perpendicular displacement field, double Bernal-stacked BLGs have a larger number of various correlated states which are tunable by an extra knob, the displacement field. Furthermore, multiple sets of flat bands due to the inherent electronic band structure of Bernal-stacked BLG may yield correlated states. The extension of twisted systems with Bernal-stacked BLGs hints us to other constituent layers, e.g., such as trilayer graphene (TLG). TLG can be found in two different stacking orders, i.e., Bernal (ABA) and rhombohedral (ABC) stacking [19–24]. Since the electronic properties are sensitive to the stacking order, a twisted system made from two TLGs is also expected to exhibit interesting electronic properties depending on the stacking order. Compared with MLG and BLG, twisted heterostructures comprised of TLG remain elusive. While recent studies on the ABC-TLG/hexagonal boron nitride (hBN) heterostructure have revealed a Mott insulator and superconductivity [25,26], less research has been focused on double TLG.

Here, we investigate magnetotransport properties of double TLG where the constituent TLGs are weakly coupled due to their large twist angle. We employed ABC-TLG as the constituent layer and the folded part of the layer, yielding ABC/CBA-type double TLG. The Landau fan diagram revealed a superposition of the constituent layers which agrees with the large twist angle (4°) from well-defined edge structure in optical microscopy. Furthermore, two distinct charge carriers were extracted, which can be attributed to one carrier pocket in the band structure of each ABC-TLG. The weakly coupled transport properties suggest that double TLG fits within the framework that describes tBLG and double BLG systems.

II. EXPERIMENTAL METHOD

The constituent ABC-TLG was exfoliated from natural graphite on SiO_2 (330 nm)/Si substrate and identified by red-filtered optical contrast imaging [Fig. 1(a)]. We utilized atomic force microscopy (AFM) with a diamond-coated tip to achieve folding, as reported previously [7], and to measure the height profile [Fig. 1(b)]. After annealing the device for 2 h with forming gas (5% H_2 and 95% N_2) at 350 °C, top contact metal electrodes (Cr/Au = 8/52 nm) were fabricated. Magnetotransport measurements were carried out in a ^{4}He superconducting magnet (1.5 K) with the DC method (500 nA bias current). Raman spectroscopic measurements were performed under ambient conditions using a 561 nm laser and a Horiba T64000 triple stage spectrometer. The laser was focused onto the sample using a 50× microscope objective (Olympus), resulting in a laser spot diameter of ∼5 μm.

*hong@nano.uni-hannover.de

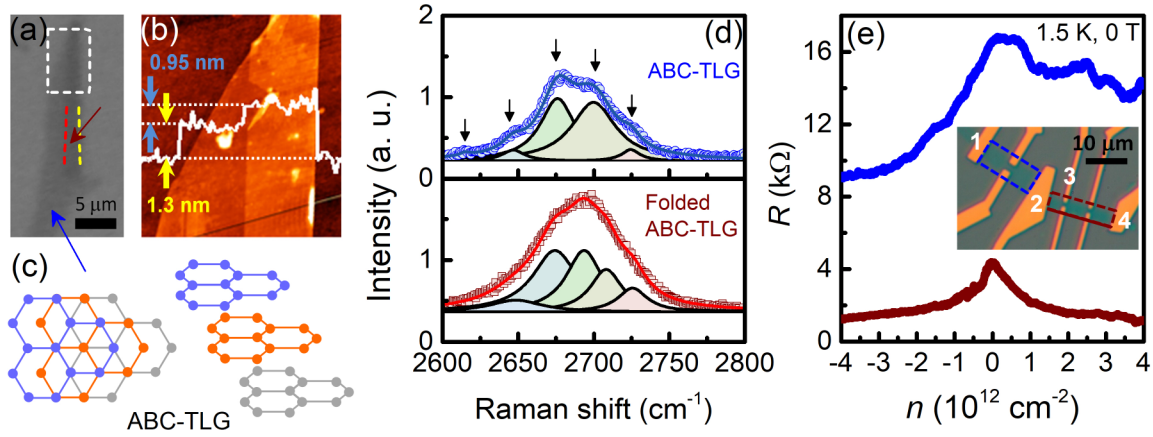

FIG. 1. (a) Optical image of ABC-trilayer graphene (TLG) (blue arrow) and its folded structure (brown arrow). The folding angle between red- and yellow-dashed lines is ∼2°, yielding its twist angle of 4°. (b) The corresponding atomic force microscopy (AFM) image of folded ABC-TLG [white-dashed box in Fig. 1(a)]. The height between TLGs is ∼0.95 nm, which is consistent with the typical height of TLG. (c) Schematic atomic structure of ABC-TLG, where top (left) and perspective (right) view are presented. (d) Raman spectra for single (top) and double (bottom) ABC-TLG. Blue circles (top) show typical shape of ABC-TLG with well-separated Lorentzian peaks. Brown squares (bottom) exhibit broadened and merged features due to interlayer interaction. Blue- and red-solid lines are fitting curves. A total of five individual Lorentzian peaks are employed for both single and double ABC-TLG. (e) R vs n plots for single (blue) and double (brown) ABC-TLG at 1.5 K and 0 T. Inset indicates an optical image of fabricated devices for single (blue-dashed box) and double (brown-dashed box) ABC-TLG, where the brown-solid line indicates folding.

III. RESULTS AND DISCUSSION

Figure 1(a) shows an optical image of ABC-TLG (blue arrow) and its folded structure (brown arrow). The typical atomic structure of ABC-TLG is schematically depicted in Fig. 1(c). We extracted a twist angle $\theta = 4^\circ$ using the folding angle $\phi = 2^\circ$ between red- and yellow-dashed lines, where the twist angle (θ) and the folding angle (ϕ) are related by $\theta = 2\phi$ [7]. In Fig. 1(b), an AFM image of the area within the white-dashed box in Fig. 1(a) can be seen. The white line in Fig. 1(b) indicates the measured height profile with step heights of 1.3 and 0.95 nm for lower and upper TLGs, respectively. With a thickness of 0.34 nm for MLG, the measured heights are consistent with the expected value of TLG considering the typical larger step height measured from the substrate.

We confirm the ABC stacking order by Raman spectroscopy, as shown in Fig. 1(d). Blue circles in Fig. 1(d) indicate the 2D peak of single ABC-TLG, showing its asymmetric shape and apparent shoulders. We fitted the 2D peak with 5 Lorentzian lines located at 2615, 2646, 2676, 2700, and 2725 cm^{-1}, which is in general agreement with previous Raman scattering results on ABC-stacked graphene [20]. While the previous studies employed a total of 6 Lorentzian lines (the feature ∼2700 cm^{-1} was described by two separate peaks) [27,28], our spectral resolution might not be sufficient to unambiguously separate these two features. Nonetheless, the overall fitting is in very good agreement with ABC-stacked graphene. In contrast, the Raman spectrum for double ABC-TLG [brown squares in Fig. 1(d)] is distinctly different. The overall shape of the 2D peak becomes more symmetric as shoulders start to overlap. We attribute this to the interaction between upper and lower TLGs with 4° of twist angle. Despite this rather symmetric line shape, employing a single Lorentzian line to describe the experimental results yields significant discrepancies between data and fit (not shown here). Instead, the 5-peak model captures the features of the Raman spectrum well, with lines centered at 2648, 2674, 2693, 2708, and 2726 cm^{-1}. Comparing single TLG to double TLG, the averaged phonon linewidth for the constituent Lorentzian peaks increases from 20.9 cm^{-1} (single TLG) to 31.1 cm^{-1} (double TLG). This broadening could be taken as further evidence for the interlayer coupling. Furthermore, the observation that the peak intensity ∼2700 cm^{-1} becomes stronger than that ∼2675 cm^{-1} in the case of double TLG hints toward a dimensional crossover from 2D to three-dimensional graphite [29,30]. In the case of tBLG or double BLG with large twist angles ∼30°, 2D peaks usually maintain the original features of the constituent layer [31,32]. Namely, while single Lorentzian (tBLG) and 4 sub-Lorentzian peaks (double BLG) are still obtained in the case of large twist angles, 2D peaks are only modified in the case of small twist angles due to interlayer interaction in such structures. Here, in our case of twisted double TLG, modifications of Raman spectra appear already for a larger twist angle.

In addition to the 2D peak, the G peak can provide additional stacking information, as in the Supplemental Material [33] (see also Refs. [34,35] therein): namely, the peak position in ABC-TLG is reported to be relatively redshifted compared with that of ABA-TLG. In our case, folded ABC-TLG has a G peak at 1580 cm^{-1}, lower than that of single ABC-TLG at 1583 cm^{-1} (Fig. S1 in the Supplemental Material [33]). The result implies that the possibility of structural phase transition from ABC to ABA stacking order can be excluded. Rather, the redshift in folded ABC-TLG can be attributed to interlayer coupling in conjunction with the aforementioned 2D peak property.

Figure 1(e) shows carrier-density-dependent resistances (R vs n) of single (blue) and double (brown) ABC-TLG at 1.5 K and vanishing magnetic field. The carrier density n is obtained using the parallel-plate capacitor model on SiO_2 substrate,

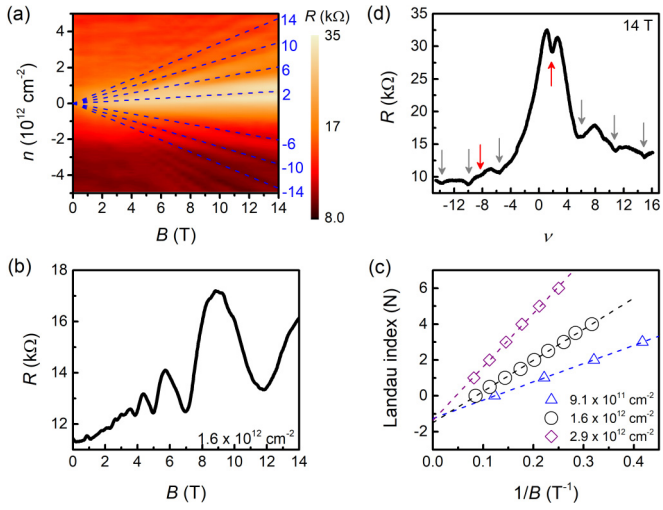

FIG. 2. (a) Landau fan diagram (R) of single ABC-trilayer graphene (TLG) at 1.5 K, showing typical filling factor $\nu = \pm 6$, ± 10, and ± 14. Additionally, $\nu = 2$ is also observed. (b) R vs B with $1.6 \times 10^{12}\,\mathrm{cm}^{-2}$. (c) Extraction of Berry phase of ABC-TLG with three carrier densities. 3π Berry phase is obtained from intercept value of -1.5 for all cases. (d) At 14 T, resistance dips are observed at the filling factor $\nu = \pm 6$, ± 10, and ± 14, as shown by gray arrows. Furthermore, there are additional signatures of $\nu = 2$ and -8, as shown by red arrows.

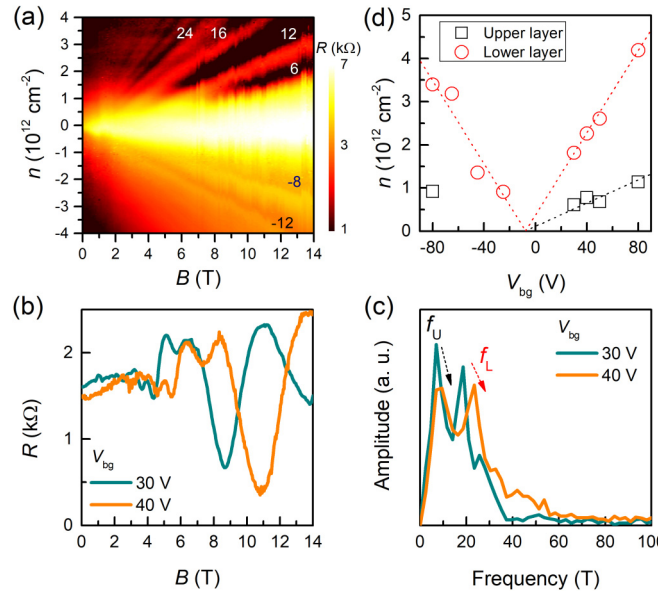

FIG. 3. (a) Landau fan diagram (R) of double ABC-trilayer graphene (TLG) at 1.5 K. (b) R vs B with $V_{bg} = 30$ and 40 V, indicating superposition of two kinds of carrier densities. (c) Fourier transform of R vs B^{-1} plot in Fig. 3(b) exhibits two distinct peaks, f_U and f_L, stemming from each carrier density of upper and lower TLG. (d) Extraction of carrier densities with different V_{bg}. Black squares and red circles are experimental results corresponding to upper and lower TLG, respectively. Guided red- and black-dotted lines are coincident around $V_{bg} = -8$ V, which is like the charge neutrality point (CNP; $V_{bg} = -5.6$ V) at 0 T.

where $n = \alpha \times (V_{bg} - V_{CNP})$ and $\alpha = 6.55 \times 10^{10}\,\mathrm{V}^{-1}\,\mathrm{cm}^{-2}$ for 330-nm-thick SiO_2. The inset of Fig. 1(e) exhibits an optical image of the fabricated devices for single (blue-dashed box) and double (brown-dashed box) ABC-TLG, where the brown-solid line indicates the folded part. Electrodes 1–4 are also marked in the inset. The resistance (R) was measured by applying the electric current from electrode 1 to 4 and analyzing the voltage drops between electrode 1 and 2 (electrode 2 and 3) for single (double) ABC-TLG, respectively, resulting in 3-terminallike measurements of the single layer and 4-terminallike measurements of the double layer. The asymmetry of the measured carrier-density-dependent resistance curves and the additional features appearing there are attributed to the influence of the field effect to the trilayer structures.

To analyze the electronic properties of the devices in more detail, Fig. 2 exhibits magnetotransport results of the single ABC-TLG device. The resistance (R) shows a typical sequence (± 6, ± 10, ± 14, and so on) of filling factors (ν) in the Landau fan diagram, as shown in Fig. 2(a). Furthermore, the fact that the Landau fan diagram originates at a single point of coincidence [charge neutrality point (CNP)] also confirms the ABC stacking order. For ABA-type structures, it has been observed that monolayerlike and bilayerlike dispersions are superimposed (i.e., linear and parabolic dispersion) [19,20,22–24]. In our single ABC-TLG device, the Landau fan does not consist of monolayerlike and bilayerlike dispersion excluding the ABA stacking order. For a carrier density of $n = 1.6 \times 10^{12}\,\mathrm{cm}^{-2}$, the resistance R shows pronounced Shubnikov–de Haas (SdH) oscillations, as seen in Fig. 2(b), with clear minima for filling factors 6, 10, 14, and 18. For TLG, the filling factor ν is connected to the Landau-level index N via $\nu = 4(\mathrm{N} + \frac{3}{2})$. In Fig. 2(c), we plot the Landau index (N) as a function of B^{-1} for different carrier densities. The obtained indices can be fitted by linear functions for the individual densities, yielding intercept values around -1.5 for all three densities. Intercept values in such plots can be regarded as direct indications of the Berry phase. As a result, 0.5 and 0 values have been obtained in MLG and Bernal-stacked BLG for the π [36,37] and 2π [38] Berry phases, respectively. Likewise, the -1.5 intercept value in TLG stands for the 3π Berry phase [21]. By looking in more detail at the measured resistance, we can see weak minima not described by filled Landau levels. In Fig. 2(d), the measured resistance R is plotted vs ν at 14 T. Local dips are observed at typical ν values of ABC-TLG, as indicated by gray arrows and as discussed above. In addition, we can see a clear minimum for $\nu = 2$ and a weak minimum at $\nu = -8$ (both indicated by red arrows) and a dip close to $\nu = 8$. Interestingly, there is no clear minimum at $\nu = -2$ observed. It seems to be hidden in the much steeper decrease of the resistance on the hole side in going away from the CNP in comparison with the electron side. This asymmetry indicates the asymmetric doping due to the back gate. The observed additional minima must be attributed to broken symmetry states being strongest in the lowest Landau levels [39].

In coming now to the twisted structure, Fig. 3(a) shows the Landau fan diagram (R) of double ABC-TLG. Before substantial discussion, it is worth confirming that the ABC stacking order is maintained during the folding process. As a control

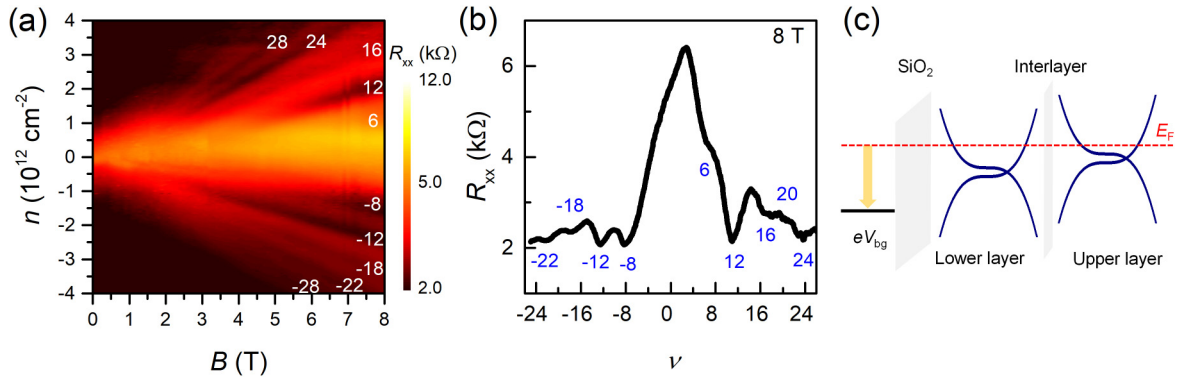

FIG. 4. (a) Landau fan diagram (R_{xx}) of double ABC-trilayer graphene (TLG) at 1.5 K. (b) R_{xx} vs ν at 8 T. Each R_{xx} dip matches with summation of two filling factors from upper and lower TLG. (c) Schematic band diagram of double ABC-TLG at 0 T.

experiment, we constructed weakly coupled ABA-TLG with a twist angle of ∼26° [33]. The Landau fan diagram apparently exhibits a superposition of monolayerlike and bilayerlike dispersion from each TLG layer, which is distinguished from Fig. 3(a). Therefore, the Landau fan diagram in Fig. 3(a) confirms the ABC stacking order consistent with the Raman spectroscopy study.

The absence of any satellite structure in the Landau fan indicates that the twist angle of 4° seems to be out of carrier density range, namely, larger V_{bg} is necessary to observe the satellite Landau fan. This observation is consistent with previous reports where tBLG exhibits typically only weak interlayer coupling in the case of twist angles >3° [6,7]. Moreover, the Landau fan shows an asymmetry with respect to the observed filling factors between the electron and hole sides, which we attribute to the influence of independent doping of upper and lower TLGs and their superposition. The superposition of two kinds of carriers originating from each TLG can be further confirmed by the investigation of SdH oscillations, as shown in Fig. 3(b). With fixed $V_{bg} = 30$ and 40 V, each resistance trace R shows magnetic-field-dependent oscillations which stem from two distinct charge carriers. To extract the two carrier densities due to upper and lower TLGs (n_U and n_L), we carried out Fourier transform (FT) from the R vs B^{-1} plot [Fig. 3(c)]. In both cases of $V_{bg} = 30$ and 40 V, two distinct peaks (f_U and f_L) can be seen. With increasing V_{bg}, the peaks move toward higher frequencies, corresponding to higher carrier densities, namely, $n_{U,L} = f_{U,L} \times 4e/h$ can be calculated. Compared with f_L, f_U changes less, which is attributed to the screening of the upper TLG by the lower TLG. We repeated the same analysis for different V_{bg}. As a result, we obtain n (n_U and n_L) vs V_{bg}, as shown in Fig. 3(d). Here, n_U and n_L are depicted by black squares and red circles, respectively. The extracted carrier densities on both the electron and hole sides show a similar behavior, as indicated by the dotted lines. The coincident position ($V_{bg} = -8$ V) is reasonably consistent for all the lines and close to the observed CNP ($V_{bg} = -5.6$ V) at 0 T. Furthermore, the common coincidence between upper and lower TLGs indicates that a potential difference between upper and lower TLGs at 0 T is negligible for the twisted structure.

Interestingly, the screening effect of the lower TLG seems to be less than observed for MLG; in other words, the ratio of induced charge carrier densities between the lower and upper layers is larger in tBLG [1]. Previously, it has been reported that the screening effect increases with the number of graphene layers, which is the opposite tendency compared with our case here [40]. In our case, the distance between the TLG layers must be considered. In addition, the electronic compressibility and especially the influence of the twist angle on the electronic structure should be included to obtain a precise understanding of the screening effect here. Indeed, the theoretical finding that interlayer coupling enhances the screening effect [41] might provide a hint to understand our results, and consequently, further investigations regarding screening of various constituent layers with twist angles are highly desired.

To analyze the Landau fan in more detail, R_{xx} was studied up to 8 T, as shown in Fig. 4(a). For our pseudo-4-terminal device the Hall contribution can be subtracted by considering the different magnetic field polarities. Then R_{xx} can be obtained via $R_{xx} = \frac{R(+B)+R(-B)}{2}$. Although the obtained R_{xx} basically includes similar information to R in Fig. 3(a), Landau levels with high indexes in Fig. 4(a) are more clearly shown due to removal of transverse contribution and the usage of additional data. Figure 4(b) shows R_{xx} calculated in this way vs ν at a magnetic field of 8 T. The local minima corresponding to different ν, as observed in Fig. 4(a), reveal again the asymmetric ν sequences between the electron and hole sides. The electron side shows $\nu = 6$, 12, 16, 20, and 24, which can be understood by the asymmetric doping between upper and lower TLGs. As in tBLG and double BLG, the asymmetric doping can be attributed to the modulation of the charge carrier density only by one gate, here, the bottom gate (V_{bg}). In this light, we draw a band diagram without magnetic field in Fig. 4(c), where two cubic dispersions are present on the SiO_2 substrate and separated by interlayer dielectric material. As we apply V_{bg}, the two TLGs are differently doped due to the screening by the lower layer. As a result, we can identify $\nu = 6$, 12, 16, 20, and 24 as $(\nu_L, \nu_U) = (6, 0), (6, 6), (10, 6), (10, 10)$, and (14, 10), where ν_L and ν_U are filling factors for lower and upper TLGs, respectively. In the case of the hole side, the sequence of prominent filling factors looks different. The broken symmetry states ($\nu = -2$ and -8) from single TLG seem to be important to account for the ν sequence. We may attribute $\nu = -8$, -12, -18, and -22 to $(\nu_L, \nu_U) = (-6, -2), (-6, -6), (-10, -8)$, and $(-14, -8)$. The filling factor selection for each layer must be consistent with the

band diagram, as shown in Fig. 4(c), namely, the upper TLG is less doped by the bottom gate because of screening of the lower TLG. Furthermore, broken symmetry states ($\nu = -2$ and -8) in the upper TLG can be realized with the help of the lower TLG as an ideal substrate like hBN, i.e., leading to a higher mobility and quality for the upper layer. From these observations, the prevalence of broken symmetry states in the filling factor sequence for the upper layer could be understood for the hole side. The absence of broken symmetry states on the electron side is less obvious in this respect and remains a puzzling fact.

Finally, we discuss the role of the fold in the folded ABC-TLG. Previously, we reported that folding induces electron doping due to compressive strain and that a structure being independent of the applied perpendicular magnetic field [18] is observed in magnetotransport. In that regard, both such features can be seen at $n \approx -7.5 \times 10^{11}\,\mathrm{cm}^{-2}$: namely, a humplike structure in Fig. 1(e) and independence of magnetic field in Fig. 4(a), respectively. In fact, a more precise carrier density for the strain-induced doping at the fold n_{fold} should be obtained by considering the back gate capacitance and V_{bg} for the fold, namely, $V_{\mathrm{bg}} = -15.5$ V for the folded structure (CNP is around -5.4 V.) yields $n \approx -10 \times 10^{11}\,\mathrm{cm}^{-2}$ for the strain-induced doping. This result agrees with previous observations in terms of electron doping and twist angle dependence [18].

IV. SUMMARY

In summary, we have investigated magnetotransport properties of double ABC-TLG where the two constituent TLGs are twisted by 4°. ABC stacking order was confirmed by Raman spectroscopy and the Landau fan diagram of the single TLG. In the case of twisted double ABC-TLG, the Raman spectrum is modified, confirming that the adjacent layers interact. In the Landau fan diagram of the double ABC-TLG superlattice structure, an asymmetric filling is seen. Furthermore, we observe the superposition of two distinct kinds of carriers in the SdH oscillations from which the two charge carrier densities are extracted. The differences are attributed to screening of the upper layer by the lower one. Due to this screening, broken symmetry states appear preferentially in the upper layer. We have expanded here the current framework for understanding and describing twistronics using ABC-TLG. As a result, electronic structures and correlated states are envisioned based on more complicated constituent graphene layers.

ACKNOWLEDGMENTS

This paper is supported by the Deutsche Forschungsgemeinschaft under Germany's Excellence Strategy-EXC 2123 Quantum Frontiers–390837967 and within priority program SPP 2244 "2DMP," by the state of Lower Saxony via the School for Contacts in Nanosystems and Fundamentals of Physics and Metrology Initiative. Part of the work in this paper has been performed using facilities at the LNQE, Leibniz Universität Hannover, Germany. S.J.H. also acknowledges support from the National Research Foundation of Korea grant funded by the Korean government (NRF-2019R1I1A1A01058123 and NRF-2021R1A4A5031762). P.L. and D.W. acknowledge support from QUANOMET-NL4 and the Institute for Basic Science (IBS-R009-Y3).

[1] H. Schmidt, T. Lüdtke, P. Barthold, E. McCann, V. I. Fal'ko, and R. J. Haug, Appl. Phys. Lett. **93**, 172108 (2008).
[2] H. Schmidt, T. Lüdtke, P. Barthold, and R. J. Haug, Phys. Rev. B **81**, 121403(R) (2010).
[3] J. D. Sanchez-Yamagishi, T. Taychatanapat, K. Watanabe, T. Taniguchi, A. Yacoby, and P. Jarillo-Herrero, Phys. Rev. Lett. **108**, 076601 (2012).
[4] B. Fallahazad, Y. Hao, K. Lee, S. Kim, R. S. Ruoff, and E. Tutuc, Phys. Rev. B **85**, 201408(R) (2012).
[5] S. J. Hong, J. A. Rodríguez-Manzo, K. H. Kim, M. Park, S. J. Baek, D. I. Kholin, M. Lee, E. S. Choi, D. H. Jeong, D. A. Bonnell *et al.*, Synth. Met. **216**, 65 (2016).
[6] Y. Kim, J. Park, I. Song, J. M. Ok, Y. Jo, K. Watanabe, T. Taniquchi, H. C. Choi, D. S. Lee, S. Jung *et al.*, Sci. Rep. **6**, 38068 (2016).
[7] H. Schmidt, J. C. Rode, D. Smirnov, and R. J. Haug, Nat. Commun. **5**, 5742 (2014).
[8] Y. Kim, P. Herlinger, P. Moon, M. Koshino, T. Taniguchi, K. Watanabe, and J. H. Smet, Nano Lett. **16**, 5053 (2016).
[9] Y. Cao, J. Y. Luo, V. Fatemi, S. Fang, J. D. Sanchez-Yamagishi, K. Watanabe, T. Taniguchi, E. Kaxiras, and P. Jarillo-Herrero, Phys. Rev. Lett. **117**, 116804 (2016).
[10] K. Kim, A. DaSilva, S. Huang, B. Fallahazad, S. Larentis, T. Taniguchi, K. Watanabe, B. J. LeRoy, A. H. MacDonald, and E. Tutuc, Proc. Natl. Acad. Sci. USA **114**, 3364 (2017).
[11] T.-F. Chung, Y. Xu, and Y. P. Chen, Phys. Rev. B **98**, 035425 (2018).
[12] Y. Cao, V. Fatemi, S. Fang, K. Watanabe, T. Taniguchi, E. Kaxiras, and P. Jarillo-Herrero, Nature (London) **556**, 43 (2018).
[13] Y. Cao, V. Fatemi, A. Demir, S. Fang, S. L. Tomarken, J. Y. Luo, J. D. Sanchez-Yamagishi, K. Watanabe, T. Taniguchi, E. Kaxiras *et al.*, Nature (London) **556**, 80 (2018).
[14] S. Carr, D. Massatt, S. Fang, P. Cazeaux, M. Luskin, and E. Kaxiras, Phys. Rev. B **95**, 075420 (2017).
[15] Y. Cao, D. Rodan-Legrain, O. Rubies-Bigorda, J. M. Park, K. Watanabe, T. Taniguchi, and P. Jarillo-Herrero, Nature (London) **583**, 215 (2020).
[16] X. Liu, Z. Hao, E. Khalaf, J. Y. Lee, Y. Ronen, H. Yoo, D. H. Najafabadi, K. Watanabe, T. Taniguchi, A. Vishwanath *et al.*, Nature (London) **583**, 221 (2020).
[17] G. W. Burg, J. Zhu, T. Taniguchi, K. Watanabe, A. H. MacDonald, and E. Tutuc, Phys. Rev. Lett. **123**, 197702 (2019).
[18] S. J. Hong, X. Xiao, D. Wulferding, C. Belke, P. Lemmens, and R. J. Haug, 2D Mater. **8**, 045009 (2021).

[19] T. Taychatanapat, K. Watanabe, T. Taniguchi, and P. Jarillo-Herrero, Nat. Phys. **7**, 621 (2011).
[20] W. Bao, L. Jing, J. Velasco Jr, Y. Lee, G. Liu, D. Tran, B. Standley, M. Aykol, S. B. Cronin, D. Smirnov *et al.*, Nat. Phys. **7**, 948 (2011).
[21] L. Zhang, Y. Zhang, J. Camacho, M. Khodas, and I. Zaliznyak, Nat. Phys. **7**, 953 (2011).
[22] S. H. Jhang, M. F. Craciun, S. Schmidmeier, S. Tokumitsu, S. Russo, M. Yamamoto, Y. Skourski, J. Wosnitza, S. Tarucha, J. Eroms *et al.*, Phys. Rev. B **84**, 161408(R) (2011).
[23] E. A. Henriksen, D. Nandi, and J. P. Eisenstein, Phys. Rev. X **2**, 011004 (2012).
[24] K. Zou, F. Zhang, C. Clapp, A. H. MacDonald, and J. Zhu, Nano Lett. **13**, 369 (2013).
[25] G. Chen, L. Jiang, S. Wu, B. Lyu, H. Li, B. L. Chittari, K. Watanabe, T. Taniguchi, Z. Shi, J. Jung *et al.*, Nat. Phys. **15**, 237 (2019).
[26] G. Chen, A. L. Sharpe, P. Gallagher, I. T. Rosen, E. J. Fox, L. Jiang, B. Lyu, H. Li, K. Watanabe, T. Taniguchi *et al.*, Nature (London) **572**, 215 (2019).
[27] L. M. Malard, M. A. Pimenta, G. Dresselhaus, and M. S. Dresselhaus, Phys. Rep. **473**, 51 (2009).
[28] C. Cong, T. Yu, K. Sato, J. Shang, R. Saito, G. F. Dresselhaus, and M. S. Dresselhaus, ACS Nano **5**, 8760 (2011).
[29] E. B. Barros, N. S. Demir, A. G. Souza Filho, J. Mendes Filho, A. Jorio, G. Dresselhaus, and M. S. Dresselhaus, Phys. Rev. B **71**, 165422 (2005).
[30] B. H. Kim, S. J. Hong, S. J. Baek, H. Y. Jeong, N. Park, M. Lee, S. W. Lee, M. Park, S. W. Chu, H. S. Shin *et al.*, Sci. Rep. **2**, 690 (2012).
[31] K. Kim, S. Coh, L. Z. Tan, W. Regan, J. M. Yuk, E. Chatterjee, M. F. Crommie, M. L. Cohen, S. G. Louie, and A. Zettl, Phys. Rev. Lett. **108**, 246103 (2012).
[32] Y. Y. Wang, J. Jiang, C. W. Gao, H. Y. Nan, Z. H. Ni, D. Wang, B. Zhong, and G. W. Wen, J. Raman Spectrosc. **47**, 668 (2016).
[33] See Supplemental Material at http://link.aps.org/supplemental/10.1103/PhysRevB.105.205404 for (a) Raman G peak of ABA-TLG and folded ABC-TLG, (b) Landau fan diagram of double ABA-TLG with twist angle of 26°, and (c) Transverse resistance of double ABC-TLG.
[34] J. Zhang, J. Han, G. Peng, X. Yang, X. Yuan, Y. Li, J. Chen, W. Xu, K. Liu, Z. Zhu *et al.*, Light Sci. Appl. **9**, 174 (2020).
[35] K. Park and S. Ryu, Sci. Rep. **5**, 8707 (2015).
[36] K. S. Novoselov, A. K. Geim, S. V. Morozov, D. Jiang, M. I. Katsnelson, I. V. Grigorieva, S. V. Dubonos, and A. A. Firsov, Nature (London) **438**, 197 (2005).
[37] Y. Zhang, Y.-W. Tan, H. L. Stormer, and P. Kim, Nature (London) **438**, 201 (2005).
[38] K. S. Novoselov, E. McCann, S. V. Morozov, V. I. Fal'ko, M. I. Katsnelson, U. Zeitler, D. Jiang, F. Schedin, and A. K. Geim, Nat. Phys. **2**, 177 (2006).
[39] L.-J. Yin, L.-J. Shi, S.-Y. Li, Y. Zhang, Z.-H. Guo, and L. He, Phys. Rev. Lett. **122**, 146802 (2019).
[40] N. J. Lee, J. W. Yoo, Y. J. Choi, C. J. Kang, D. Y. Jeon, D. C. Kim, S. Seo, and H. J. Chung, Appl. Phys. Lett. **95**, 222107 (2009).
[41] J. M. Pizarro, M. Rösner, R. Thomale, R. Valentí, and T. O. Wehling, Phys. Rev. B **100**, 161102(R) (2019).